A global evaluation of the regional spatial variability of column integrated CO_2 distributions

Alanood A. Alkhaled,[1] Anna M. Michalak,[1,2] S. Randolph Kawa,[3] Seth C. Olsen,[4] and Jih-Wang Wang[5]

[1]   Satellites, such as the Orbiting Carbon Observatory (OCO), are expected to provide global measurements of column-averaged carbon dioxide (CO_2) dry-air mole fraction (X_{CO2}) with the potential of improving the scientific understanding of regional carbon cycle processes and budgets. The satellite data products, however, are expected to have large data gaps due to the satellite track and geophysical limitations (e.g., clouds and aerosols). The satellite data will also be representative of the X_{CO2} distribution at the spatial scale of satellite footprints, which is smaller than the resolution of typical transport or process models. Assessing the ability of the retrieved soundings to capture X_{CO2} variability over different regions and times, evaluating the representation error associated with using the retrieved X_{CO2} product to represent X_{CO2} at typical model resolutions, and filling data gaps while providing an estimate of the associated uncertainty all require the evaluation of the spatial variability of X_{CO2}. In this study, the global spatial covariance structure of X_{CO2} is evaluated regionally using CO_2 concentrations simulated using the MATCH/CASA model. Results show that regional and temporal changes in the X_{CO2} distribution caused by seasonal changes in surface fluxes and transport produce a spatially and temporally variable X_{CO2} covariance structure. The effects of model setup and the relatively low resolution of the MATCH/CASA model on the evaluated X_{CO2} covariance structure are assessed by comparing the MATCH/CASA results to the spatial variability inferred from the higher-resolution PCTM/GEOS-4 global model, the SiB-RAMS regional model, and aircraft campaign point observations. The comparison with the higher-resolution models and aircraft data shows good agreement with MATCH/CASA results, thus indicating that the presented results provide an adequate representation of X_{CO2} variability as will be measured by satellites such as OCO.

1. Introduction

[2]   Predicting future changes in the Earth's climate due to increasing carbon dioxide (CO_2) concentrations depends on understanding and accurately modeling the physical processes controlling the carbon cycle. Achieving these objectives requires the availability of dense, globally distributed measurements of atmospheric CO_2 concentrations, which could be used to infer CO_2 sources and sinks

at regional scales. The existing CO_2 measurement network [*GLOBALVIEW-CO2*, 2005], however, is too sparse to achieve this goal. A main component of the efforts to overcome this limitation is the launch of satellite missions, such as the Orbiting Carbon Observatory (OCO) [*Crisp et al.*, 2004; *Miller et al.*, 2007] and the Greenhouse Gases Observations Satellite (GOSAT) [*National Institute for Environmental Studies*, 2006] to provide global coverage of high-density measurements of column-averaged CO_2 dry-air mole fraction (X_{CO2}) at regional precisions of 1 ppm [*Crisp et al.*, 2004; *Chevallier et al.*, 2007].

[3]   Satellite measurements, however, are expected to have large data gaps, and to be representative of spatial scales that are much smaller than the spatial resolution of typical global models used in the estimation of CO_2 sources and sinks. Evaluating the information content, uncertainties, and errors associated with gap-filled satellite data products requires a quantification of the spatial and temporal scales of variability of X_{CO2}, and an analysis of how this variability itself varies between regions and across

[1]Department of Civil and Environmental Engineering, University of Michigan, Ann Arbor, Michigan, USA.
[2]Also at Department of Atmospheric, Oceanic and Space Sciences, University of Michigan, Ann Arbor, Michigan, USA.
[3]NASA Goddard Space Flight Center, Greenbelt, Maryland, USA.
[4]Los Alamos National Laboratory, Los Alamos, New Mexico, USA.
[5]Cooperative Institute for Research in the Environmental Sciences and Department of Atmospheric and Oceanic Sciences, University of Colorado, Boulder, Colorado, USA.

seasons because of changes in CO_2 fluxes and transport pathways.

[4] Large data gaps in satellite measurements over various regions and times are caused by geophysical limitations such as clouds and aerosols, and the limited satellite track [*Buchwitz et al.*, 2005; *Engelen and McNally*, 2005; *Barkley et al.*, 2006a; *Bösch et al.*, 2006; *Tiwari et al.*, 2006; *Miller et al.*, 2007]. For example, *Bösch et al.* [2006] reported that the number of viable SCIAMACHY X_{CO2} retrievals over North America in April and May 2005 using a strict cloud filter was only 5% of the total number of soundings. Understanding of the spatial covariance structure of X_{CO2}, which quantifies X_{CO2} variability, is necessary for evaluating the ability of the retrieved fraction of soundings to capture the underlying X_{CO2} distribution. The quantification of global variability at regional scales will also facilitate the use of optimal spatial interpolators (e.g., kriging) that not only provide gap-filled global X_{CO2} maps, but also provide a measure of gap-filling uncertainty. These maps are important for validating transport models and can play a key role in the validation of estimated CO_2 sources and sinks.

[5] Similarly, knowledge of X_{CO2} regional spatial variability would be necessary for identifying satellite soundings that provide the best characterization of the underlying X_{CO2} distribution, by focusing more resources on areas with higher variability. Such sounding selection may be required in early stages of the OCO mission, to manage the high computational costs associated with processing the expected massive data volumes.

[6] The evaluation of representation errors associated with using satellite measurements to represent the X_{CO2} distribution at coarser resolution also requires the evaluation of X_{CO2} variability at regional scales. These errors result from the mismatch in spatial scale between the satellite measurement resolution (e.g., OCO soundings will have an approximately 3 km^2 footprint) and the resolution of typical atmospheric transport models or general circulation models (i.e., $100-1000$ km) used in determining CO_2 sources and sinks [*Miller et al.*, 2007; *Corbin et al.*, 2008]. Estimates of the regional spatial variability of X_{CO2} can be used to statistically quantify representation errors [*Alkhaled et al.*, 2008]. For example, over areas with low spatial variability, retrieved soundings will be more representative of the average X_{CO2} over a model grid cell, and will therefore have lower representation errors relative to areas with high spatial variability.

[7] The overall objective of this paper is to analyze the current understanding of the spatial variability of X_{CO2}, as simulated by current models, at global and regional scales. The presented analysis quantifies monthly X_{CO2} variability using spatial covariance parameters that represent the global and regional spatial variability of simulated X_{CO2} fields. Preliminary results presented by *Miller et al.* [2007] established the need for such analysis. This paper quantifies the spatial variability of X_{CO2}, and attributes observed seasonal and regional differences to variability in surface fluxes and seasonal changes in global transport. Results of this study provide an understanding of the expected information content of soundings retrieved by future satellites.

[8] The paper is organized as follows. Section 3 describes the examined models and analysis methods. The results of the spatial variability analysis are presented in section 4. On the global scale, section 4.1 presents daily spatial variability parameters to investigate the overall seasonality of X_{CO2} variability. Following the global-scale analysis, monthly regional-scale spatial covariance parameters are quantified in section 4.2 to identify the local variability over different regions. The effects of using low-resolution X_{CO2} simulations to infer X_{CO2} spatial variability are evaluated in section 4.3 through comparison with higher-resolution models and aircraft data. A summary of the main conclusions of the study are presented in section 5.

2. Background

[9] Contrary to the relatively extensive literature analyzing the variability of surface CO_2 concentrations [*Conway et al.*, 1994; *Randerson et al.*, 1997; *Geels et al.*, 2004; *Nicholls et al.*, 2004; *Lu et al.*, 2005; *Wang et al.*, 2007], the spatial and temporal variability of X_{CO2} is the focus of only a limited number of studies. In general, these studies have focused on two main areas: (1) determining the type of information that X_{CO2} measurements can provide relative to surface concentrations and, therefore, their value to carbon cycle research and (2) evaluating the ability of retrievals from existing satellites to capture the spatial and temporal variability of X_{CO2}, by comparing satellite retrievals to model simulations and/or surface-based Fourier Transform Infrared Spectroscopy (FTS) measurements.

[10] Studies focusing on the first area show that X_{CO2} has lower spatial and temporal variability, and delayed response to surface disturbances, relative to surface concentrations, with delays reaching several weeks [*Olsen and Randerson*, 2004; *Warneke et al.*, 2005]. More specifically, these studies show that column-averaged volume mixing ratios reflect the spatial and temporal variability of surface CO_2 concentrations diluted by less variable concentrations beyond the Planetary Boundary Layer (PBL) [*Kawa et al.*, 2004; *Olsen and Randerson*, 2004]. The low variability of column-averaged volume mixing ratios is caused by the vertical and horizontal mixing of CO_2 concentrations throughout the column, which smoothes surface flux signals, thus leading to high precision requirements for X_{CO2} if they are to be useful in carbon cycle studies.

[11] The utility of X_{CO2} to carbon cycle science has been demonstrated by a number of studies. *Rayner and O'Brien* [2001] noted that the variability characteristics of X_{CO2} over high-convection tropical regions can be useful for determining CO_2 fluxes because the rapid vertical mixing reduces the spatial smearing of surface fluxes. Moreover, a few studies have pointed to the role of global transport in determining X_{CO2} variability in the middle to upper troposphere [*Tiwari et al.*, 2006] and the lower troposphere, particularly in the Southern Hemisphere (SH) pole region [*Nevison et al.*, 2008]. The understanding of the influence of global transport on X_{CO2}, and the large spatial footprint of fluxes influencing local X_{CO2} variability, make X_{CO2} an important quantity for identifying the relative contribution of oceanic versus terrestrial fluxes to CO_2 variability over the SH [*Nevison et al.*, 2008].

[12] Studies focusing on the second area evaluate the ability of satellites (e.g., AIRS, SCIAMACHY) to capture the spatial and temporal variability of X_{CO2}. These studies show that retrieved soundings that are uncontaminated by

aerosol or clouds are capturing the general spatial patterns of X_{CO2} over examined regions [*Barkley et al.*, 2006a, 2006b]. *Tiwari et al.* [2006] noted that there is good agreement in the amplitude of the middle to high tropospheric CO_2 subcolumn observed by AIRS and predicted by models. However, there are some differences in the phase of the observed and modeled seasonal cycle. Literature analyzing SCIAMACHY retrievals shows that the monthly means of X_{CO2} retrievals (averaged over some spatial domain) have a large spread, and that the amplitude of their seasonal cycle over the Northern Hemisphere (NH) is lower than that observed using FTS measurements [*Barkley et al.*, 2007; *Buchwitz et al.*, 2007; *Schneising et al.*, 2008], but higher than that represented by atmospheric models [*Barkley et al.*, 2006b; *Bösch et al.*, 2006]. Although reasons for the weak X_{CO2} seasonal cycle in atmospheric models were not identified in studies comparing models to satellite retrievals [*Barkley et al.*, 2006b; *Bösch et al.*, 2006], a number of studies attributed this underestimation to modeling uncertainties in the specifications of surface fluxes, errors in mixing parameterization, unrealistic stratospheric influence on simulated mixing ratios, and differences in meteorology [*Shia et al.*, 2006; *Stephens et al.*, 2007; *Washenfelder et al.*, 2006; *Yang et al.*, 2007].

[13] The spatial variability of X_{CO2} has been quantified using the spatial autocorrelation of aircraft measurements of partial columns of X_{CO2} [*Gerbig et al.*, 2003a; *Lin et al.*, 2004a], although the analysis covered only a small number of regions with limited spatial and temporal coverage. This limited knowledge about the spatial variability of X_{CO2} cannot be used to determine the information content of the global X_{CO2} measurements that will be provided by OCO, which may vary both regionally and seasonally. Similarly, the current network of high-resolution solar absorption spectrometers (FTS) (Total Carbon Column Observing Network (TCCON), http://www.tccon.caltech.edu) has only a few stations globally. Currently available satellite remote sensing data, on the other hand, have relatively low precision and large data gaps, particularly on daily time scales [*Buchwitz et al.*, 2005; *Barkley et al.*, 2006b; *Tiwari et al.*, 2006]. These data do not provide the coverage or spatial density needed for a seasonal variability analysis on a global scale.

[14] Therefore, prior to the launch of the OCO and GOSAT satellites, the global X_{CO2} spatial variability must be estimated using simulated X_{CO2}. This study provides an analysis of both the global and regional monthly X_{CO2} variability as simulated by current models.

3. Methods

[15] This section introduces the models used to simulate the analyzed X_{CO2} data, as well as the approach used to quantify spatial variability. Section 3.1 describes the MATCH/CASA model used for the main variability analysis. Methods used to quantify the spatial variability of X_{CO2} are presented in section 3.2. Finally, section 3.3 introduces models and aircraft data used to (1) validate results obtained using the MATCH/CASA model and (2) test the robustness of the inferred X_{CO2} variability to differences in model setup and resolution.

3.1. MATCH/CASA Model

[16] The analysis of the spatial variability of X_{CO2} is performed using data from the MATCH/CASA coupled biosphere transport model. The analyzed MATCH simulation has a 2-hourly temporal resolution (averaged from 30 min time steps) and a horizontal resolution of approximately $5.5° \times 5.5°$ with 26 vertical layers starting at the surface and ending at 60 km in altitude [*Olsen and Randerson*, 2004]. The CO_2 concentrations at the different model altitude layers are pressure-averaged to obtain column-integrated CO_2 concentrations (X_{CO2}). MATCH uses archived meteorological fields derived from the NCAR Community Climate Model version 3 that are representative of a climatologically average year. For the data used in this study, MATCH simulates atmospheric CO_2 resulting from three types of fluxes: (1) linearly interpolated monthly means of oceanic fluxes derived from pCO_2 measurements [*Takahashi et al.*, 1999], (2) anthropogenic emissions from *Andres et al.* [1996] uniformly distributed throughout the year, and (3) diurnally varying net ecosystem production (NEP) fluxes based on monthly net primary production (NPP) values from the CASA model [*Randerson et al.*, 1997] distributed diurnally according to shortwave radiation and temperature from the National Center for Environmental Prediction (NCEP) for the year 2000.

[17] X_{CO2} data corresponding to 1300 local time are selected to approximate the spatial variability as would be observed by OCO [*Crisp et al.*, 2004; *Miller et al.*, 2007]. The regional spatial variability of X_{CO2} is evaluated for the 15th of each month, which is assumed to represent typical variability that would be observed during an individual day in each month. Note that we are interested in the variability as will be observed by OCO, which is why the analysis is performed on a series of individual days, rather than on monthly averaged X_{CO2}. The representativeness of the 15th of each month is verified by quantifying the daily spatial variability at 1300 local time for eight consecutive days during the month with the highest observed global-scale change in variability, as will be further described in section 4.2.3.

3.2. Spatial Variability
3.2.1. Semivariogram Model

[18] The spatial variability of X_{CO2} is quantified by modeling the semivariogram of the X_{CO2} distribution, which describes the degree to which two X_{CO2} values are expected to differ as a function of their separation distance (h). To evaluate this relationship, the raw semivariogram $\gamma(h)$ is evaluated for all pairs of X_{CO2} data:

$$\gamma(h) = \frac{1}{2}\left[X_{CO2}(x_i) - X_{CO2}(x_j)\right]^2 \qquad (1)$$

where the distance (h) between locations x_i and x_j is the great circle distance between these points on the surface of the Earth:

$$h(x_i, x_j) = r\cos^{-1}\left(\sin\phi_i\sin\phi_j + \cos\phi_i\cos\phi_j\cos(\vartheta_i - \vartheta_j)\right) \qquad (2)$$

and where (ϕ_i, ϑ_i) are the latitude and longitude of location x_i, and r is the Earth's mean radius. The semivariogram is used to model the spatial autocorrelation of X_{CO2} that is not explained by a deterministic trend in the data. Therefore, the X_{CO2} north–south gradient is estimated for each month using linear regression and subtracted from the data prior to the analysis.

[19] A theoretical variogram model is selected on the basis of the observed variability to represent the spatial autocorrelation structure. The theoretical variogram describes the decay in spatial correlation between pairs of X_{CO2} measurements as a function of physical separation distance between these measurements. The exponential semivariogram [e.g., *Cressie*, 1993] is selected here to model MATCH/CASA X_{CO2} spatial variability, based on an examination of a binned version of the raw variogram. The exponential variogram is defined as:

$$\gamma(h) = \sigma^2 \left(1 - \exp\left(-\frac{h}{L} \right) \right) \quad (3)$$

where σ^2 represents the expected variance of the difference between X_{CO2} measurements at large separation distances, and $3L$ represents the practical correlation range between X_{CO2} measurements. These parameters also define the corresponding exponential covariance function: $C(h) = \sigma^2 \exp(-h/L)$.

[20] The exponential model parameters are fitted to the raw semivariogram of the latitudinally detrended X_{CO2} data using nonlinear least squares. The fitted variogram parameters define the spatial covariance structure of the modeled X_{CO2} signal. The uncertainty of the least squares fit of the variance (σ^2) and range parameter (L) are not reported in this study because the results are based on an exhaustive sample from the simulated field, and the uncertainty resulting from limited sampling is negligible. The majority of the uncertainty associated with variogram parameters stems from assumptions about fluxes and transport, and the sensitivity to these choices is explored is sections 3.3 and 4.3.

3.2.2. Spatial Variability Analysis

[21] The global spatial variability is defined through semivariogram parameters fitted to the raw semivariogram. For each day, the raw semivariogram is constructed using detrended MATCH/CASA X_{CO2} at 1300 local time for all model grid cells. The analysis is repeated for each day of the model year to identify both the seasonal trends in global variability at daily resolution, and the relationships between these trends and seasonal changes in global CO_2 flux and transport.

[22] Regional variability in the spatial covariance structure is evaluated through localized variograms representing subareas of the global domain. This analysis requires areas (regions) large enough to capture the scales of variability within a given subdomain of the model, while at the same time small enough to reveal the characteristics of local spatial variability.

[23] A regional variability analysis with a similar methodological goal was previously adopted by *Doney et al.* [2003] to measure the mesoscale global spatial variability of satellite measurements of ocean color. In that study, daily anomalies from the monthly block mean of the natural log

of chlorophyll concentrations were used to fit spherical variograms for nonoverlapping 5° regions globally.

[24] In the case of X_{CO2}, regional covariance parameters were fit for each model grid cell, resulting in a regional spatial variability analysis at a 5.5° resolution. Because regional spatial variability may reflect global general circulation patterns as well as differences in surface fluxes between regions, correlation lengths of X_{CO2} may extend beyond individual continents or ocean basins. To account for this, the local semivariogram parameters in the current work are constructed to reflect both the local variability and its relationship to global spatial variability. First, regions are defined as overlapping 2000 km radius circles centered at each model grid cell, resulting in a total of 2048 regions covering the globe. A 2000 km radius was selected because it is sufficiently large to capture much of the variability in the vicinity of a given grid cell, while being small enough to capture regional variability in the spatial covariance structure. Second, the raw semivariogram ($\gamma_{region}(h)$) is constructed using pairs of points with one point always within the defined region ($X_{CO2}(x_{region})$) and the other either within or outside that region ($X_{CO2}(x_{region} + h)$) (see Figure 1). This approach focuses on the variability observed within each subregion, while also accounting for larger scales of variability:

$$\gamma_{region}(h) = \frac{1}{2} \left[X_{CO2}\left(x_{region}\right) - X_{CO2}\left(x_{region} + h\right) \right]^2 \quad (4)$$

Third, to emphasize the covariance of X_{CO2} within the analyzed region, weighted nonlinear least squares is used to fit the local semivariogram parameters, with higher weights assigned to points within a separation distance less than or equal to 4000 km. Numerically, correlation lengths are also restricted to a maximum of half the Earth's circumference.

[25] Conceptually, a higher variance is representative of more overall variability, as is a shorter correlation length, which is indicative of more variability at smaller scales. The parameter h_o is introduced to provide a single representation of the degree of variability observed in different regions, and to merge information about both the variance and correlation lengths of X_{CO2} variability. If we consider a single sounding at a known location, h_o is defined as the maximum distance from the sounding location at which the mean squared X_{CO2} prediction error is below a preset value, V_{max}. The mean squared prediction error is the uncertainty associated with using the sounding to predict the unknown value at a given distance away from the sounding location, using ordinary kriging. Ordinary kriging is a minimum variance unbiased interpolator that takes advantage of knowledge of the spatial covariance structure to interpolate available measurements while providing an estimate of the interpolation error [*Chiles and Delfiner*, 1999]. For an exponential variogram:

$$h_{o,\exp} = -L_R \ln\left(1 - \frac{V_{max}}{2\sigma_R^2} \right) \quad (5)$$

where σ_R^2 and L_R are the fitted regional variance and range parameter, respectively.

[26] Both a higher regional variance σ_R^2 and a shorter regional range parameter L_R lead to a decrease in the overall
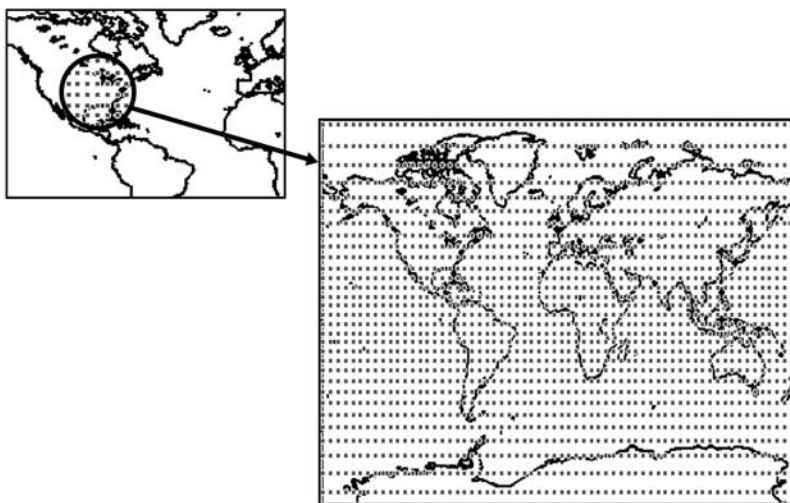
Figure 1. The regional spatial covariance evaluates the spatial variability of (left) X_{CO2} values within a region (e.g., eastern North America) and between this region and (right) global X_{CO2} values.

spatial scale over which a given measurement is representative of the surrounding X_{CO2} values. It should be noted that no measurement error is assumed in the calculation of the regional variance σ_R^2 and range parameter L_R. Therefore, the resulting h_o values demonstrate the overall spatial scale of the information provided by a noise-free X_{CO2} measurement over the measurement region and time.

[27] In subsequent sections of this work, variability inferred from the MATCH/CASA model is compared to other models and field data, where different theoretical variogram models are used to represent X_{CO2} spatial variability. Because parameters used to describe the variability differ between variogram models, the h_o parameter also provides a convenient universal metric that can be compared across models. The equivalent h_o parameters for the other variogram models used in this study are presented in subsequent sections.

[28] Conceptually, the h_o parameter can also be thought of as a measure of the expected relative spatial density of retrieved soundings that would be required to capture the spatial variability of X_{CO2} over different regions. The choice of V_{max} is somewhat flexible, but should represent a level of interpolation uncertainty that is relevant to potential applications of the data. In the presented results, V_{max} is chosen to be 0.25 ppm^2 ($\sqrt{V_{max}} = 0.5$ ppm). This level is comparable to the 1 ppm regional-scale uncertainty described as a goal for OCO [*Chevallier et al.*, 2007]. It should be noted that V_{max} represents the interpolation uncertainty assuming no measurement error. Thus, the lower variance was chosen to compensate for the additional uncertainty that would be contributed by measurement errors and other sources of error.

3.3. Comparison to Other Models and Aircraft Data

[29] The regional spatial covariance parameters inferred from the MATCH/CASA model are compared to higher-resolution models and aircraft data. The objective of this comparison is to assess the effect of model setup and resolution on inferred spatial variability, particularly at spatial scales comparable to the measurement footprint of future satellites, and in comparison to actual X_{CO2} variability as

observed by aircraft profiles. The regional covariance structure inferred from MATCH/CASA is compared to the covariance structures predicted by the Parameterized Chemistry and Transport global Model PCTM/GEOS-4 [*Kawa et al.*, 2004], a high-resolution regional model for North America (SiB-RAMS) [*Wang et al.*, 2007], and X_{CO2} aircraft data over North America and the Pacific Ocean [*Lin et al.*, 2004a].

3.3.1. PCTM/GEOS-4 Global Model

[30] Regional spatial variability is evaluated using X_{CO2} simulated using the PCTM/GEOS-4 model [*Kawa et al.*, 2004] for the months of January, April, July and October of 2002. The objective of this comparison is to assess the impact of differences in model resolution, model winds, and transport on the observed spatial variability of modeled X_{CO2}.

[31] PCTM/GEOS-4 has a 2° latitude by 2.5° longitude resolution, and is driven by analyzed meteorological fields from NASA's Goddard Earth Observing System, version 4 (GEOS-4). The GEOS-4 fields are derived from meteorological data assimilation for 2002. The model run was spun up prior to 1998 and continued forward. Surface fluxes used in PCTM/GEOS-4 are very similar to those used in MATCH/CASA. The fossil fuel and ocean fluxes are those assembled for the TransCom-Continuous model intercomparison [*Law et al.*, 2008], which are very similar to those used in MATCH (section 3.1). The terrestrial biosphere fluxes used in PCTM were also derived from CASA monthly means (section 3.1), with 3-hourly variations imposed using the same method of *Olsen and Randerson* [2004], but for PCTM the 3-hourly variations were created using the GEOS-4 meteorological data rather than NCEP. In a separate comparison, X_{CO2} results from two PCTM simulations using CASA monthly fluxes for the same year with 3-hourly variations created using GEOS-4 versus ECMWF (from TransCom-Continuous [*Law et al.*, 2008]) were found to be very similar, suggesting that NCEP-driven results would produce the same variability observed using the model simulations used in this study.

[32] X_{CO2} output nearest 1300 local solar time is selected from hourly CTM fields. The similarity in surface fluxes

between MATCH/CASA and PCTM/GEOS-4 provides a basis for assessing differences in spatial variability resulting primarily from differences in model winds, transport, and resolution, with little influence from changes caused by different assumptions about fluxes.

3.3.2. SiB-RAMS Regional Model

[33] SiB-RAMS is a fully coupled biosphere-atmosphere regional model that predicts CO_2 spatial and temporal variations by simulating CO_2 sources and sinks [*Denning et al.*, 2003]. The SiB-RAMS data used in this study are part of a 10-day simulation of a weather front event passing over North America from 11 to 21 August 2001 [*Wang et al.*, 2007]. CO_2 concentrations are simulated at three nested grids with approximately 40 km, 10 km and 2 km spatial resolutions. The largest grid (40 km) consists of 150 × 100 cells covering a longitudinal range from 144.3°W to 51.4°W and a latitudinal range from 21.9° N to 61.9° N. The smaller grids are centered at the WLEF tower located in Chequamegon National Forest east of Park Falls-Wisconsin, and cover areas of 1500 km × 1500 km and 400 km × 400 km, respectively [see *Wang et al.*, 2007, Figure 2]. The analysis was limited to the coarsest grid, because a preliminary spatial variability analysis showed that the limited area covered by the finer grids is not sufficient to characterize X_{CO2} correlation lengths.

[34] The high resolution of the SiB-RAMS model provides an opportunity for comparing the X_{CO2} spatial variability inferred from the coarse MATCH/CASA model [*Olsen and Randerson*, 2004] to the spatial variability at spatial scales closer to OCO footprint. Additionally, the SiB-RAMS simulation did not use prescribed CO_2 fluxes; instead the fluxes were derived from local meteorological conditions, thus providing a different representation of CO_2 flux variability.

[35] The SiB-RAMS simulation includes CO_2 concentrations at 44 vertical levels from approximately 30 m up to 21 km. X_{CO2} is again obtained using pressure weighted averaging of all levels of CO_2 concentrations at 1300 local time. In addition to the spatial covariance analysis of the 21 km SiB-RAMS columns, another column value is constructed by giving the final SiB-RAMS vertical level (21 km) a weight that is proportional to an elevation increment from 21 km to 60 km to be comparable to the vertical extent of MATCH/CASA X_{CO2}. Furthermore, because of the limited latitudinal range of the SiB-RAMS simulation, the latitudinal trend is not significant and is therefore not removed.

[36] A daily raw semivariogram is calculated using X_{CO2} over the entire SiB-RAMS domain. The semivariogram model parameters are then fitted to the raw semivariogram using nonlinear least squares. A Gaussian theoretical semivariogram model [e.g., *Cressie*, 1993] was found to provide the best fit to the experimental semivariogram of SiB-RAMS,

$$\gamma(h) = \sigma^2 \left(1 - \exp\left(-\frac{h^2}{L^2} \right) \right) \qquad (6)$$

For the Gaussian variogram model, the practical correlation length is equivalent to 7/4 times the range parameter L. The

h_o parameter corresponding to this variogram model is defined as:

$$h_{o,Gauss} = \sqrt{ -L^2 \ln\left(1 - \frac{V_{max}}{2\sigma^2} \right) } \qquad (7)$$

3.3.3. Aircraft Data

[37] *Lin et al.* [2004a] evaluated the spatial variability of partial columns of atmospheric CO_2 concentrations using aircraft data from the CO_2 Budget and Rectification Airborne mission (COBRA) project over North America (NA) [*Gerbig et al.*, 2003a, 2003b; *Lin et al.*, 2004b] and from the NASA Global Tropospheric Experiment (GTE) mission for the Pacific Ocean [*McNeal*, 1983]. The results of this study are used as a comparison to the variability inferred using the models described in the previous sections.

[38] The Pacific Ocean measurements represent time periods that extend from August to October and from February to April of the years 1991 to 2001. CO_2 concentrations over North America, on the other hand, were collected only in August 2000 and June 2003. *Lin et al.* [2004a] used density-weighted CO_2 concentrations for four altitude ranges (0.15–3 km, 3–6 km, 6–9 km and <9 km). For North America, the top height of the first range (0.15–3 km) was not fixed at 3 km but varied according to the PBL height, which was determined from the characteristics of the measured CO_2 profile and auxiliary measurements, such as the vertical potential temperature, H_2O, and CO vertical profiles [*Gerbig et al.*, 2003a].

[39] *Lin et al.* [2004a] used a power variogram model [e.g., *Cressie*, 1993] to represent the spatial covariance structure of the data. The power variogram had two parameters (c_1 and λ) to represent the growth in variance as a function of separation distance, as well as a parameter (c_o) to represent the measurement error:

$$\gamma(h) = \left(c_o + \left(\frac{h}{c_1} \right)^{\lambda} \right) \qquad (8)$$

To reduce the effect of temporal variability, particularly for NA profiles that were collected during both morning and afternoon flights, *Gerbig et al.* [2003a] and *Lin et al.* [2004a] constructed the raw semivariograms using X_{CO2} pairs sampled within a 3-h window of each other.

[40] The h_o parameter corresponding to this variogram model is defined as:

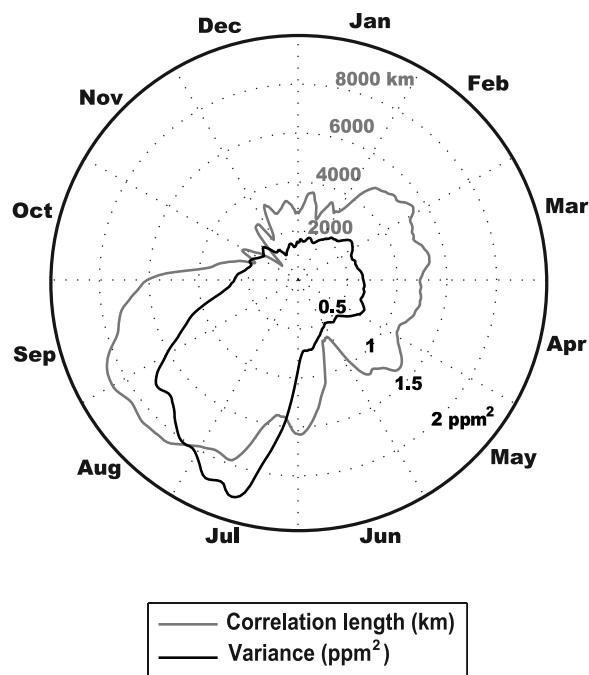$$h_{o, power} = c_1 (V_{max} - c_o)^{\frac{1}{\lambda}} \qquad (9)$$

and is evaluated for the 0.15–3 km and <9 km column heights.

4. Results and Discussion

4.1. Global X$_{CO2}$ Variability

[41] Global spatial covariance parameters inferred from the MATCH/CASA simulation show strong seasonal variability (Figure 2) that can be interpreted given known seasonal changes in CO_2 fluxes and atmospheric transport.

Figure 2. Global spatial covariance function parameters (variance and correlation length) of MATCH/CASA simulated X_{CO2} at 1300 local time evaluated daily and smoothed using a 1 week moving average.

For example, the effect of the NH growing season is demonstrated by the rapid increase in the global variance parameter starting at levels averaging between 0.3 ppm^2 and 0.75 ppm^2 in winter and spring to approximately 2.25 ppm^2 in July. The variance parameter then decreases gradually in August and rapidly in September and October, and reaches its average winter levels in November.

[42] The seasonal cycle of the variance is coupled with a similar cycle for the correlation length that follows with some lag. The correlation length cycle starts with short values during the NH winter, the values then increase during the NH spring and fall, and reach a maximum in July and September. The correlation length starts to decrease again in October to reach a minimum in November. Features of the correlation length cycle indicate that this parameter is affected by changes not only in surface fluxes, but also in seasonal transport. A clear indication of this effect is demonstrated by the sharp drop in the correlation length values in June and November. Although these drops can be related to biospheric flux changes in the NH due to the onset of NH summer and fall, changes in transport pathways and the gradual variance changes that occur around the same period indicate a possible role of transport. More specifically, this sharp decrease in both months can be attributed to seasonal changes in the location of the Intertropical Convergence Zone (ITCZ) and the associated seasonal changes in transport, particularly of the Asian and European transport pathways [Stohl et al., 2002].

[43] The ITCZ separates the high-variability X_{CO2} of the NH from the lower-variability X_{CO2} of the SH; thus, with its northward movement during the NH summer, a larger part of the Earth shows low variability. Furthermore, the movement of the ITCZ affects the seasonal transport of the X_{CO2}

signal from high-flux areas over south Asia, and to a lower degree over Africa. In winter, a large portion of the south Asian emissions are transported toward the ITCZ, while another portion is transported along with European emissions to the Arctic [Stohl, 2004]. These seasonal changes in transport affect the shape of the X_{CO2} latitudinal gradient, particularly during transition months (i.e., October–November and June–July), thus affecting the seasonal cycles of both the variance and correlation length.

[44] Other factors affecting the shape of X_{CO2} latitudinal gradient are the strong CO_2 drawdown over the NH biospherically active areas during the NH summer, coupled with the relatively high X_{CO2} values around the ITCZ regions. These factors create a nonlinear X_{CO2} gradient with a maximum either south or north of the equator depending on the location of the ITCZ, and a minimum that starts over the high latitudes in June and moves toward the midlatitudes in October. The resulting nonlinearity in the latitudinal gradient creates X_{CO2} residuals (i.e., latitudinally detrended X_{CO2}) with strong spatial continuity, evident from the variances and long correlation lengths observed in June through September.

[45] The seasonal variability of the global covariance structure, as shown in Figure 2, indicates that as expected, the NH summer months exhibit the most spatial variability. As a result, representation errors are generally expected to be higher for these months. Furthermore, discounting any differences in geophysical limitations, the uncertainty associated with gap-filled products will be higher for the summer months, and the spatial variability will be more difficult to capture. Unexpectedly, however, high variability is also observed during a NH winter month such as November, stemming from short correlation lengths, which implies that variability may be more difficult to capture during this month as well.

[46] Previous studies assessed X_{CO2} seasonal variability by calculating global, zonal or point peak-to-peak seasonal amplitudes, found to be between 6 ppm and 11 ppm at NH mid/high latitudes [Olsen and Randerson, 2004; Washenfelder et al., 2006]. Warneke et al. [2005], Bösch et al. [2006] and Washenfelder et al. [2006] indicated that models can produce a NH seasonal cycle similar to the seasonal cycle observed by FTS measurements, but with lower amplitudes. Bösch et al. [2006] also showed that there is a good qualitative agreement between the X_{CO2} seasonal cycle observed in model simulations, FTS measurements, and SCIAMACHY retrievals. More recently, Schneising et al. [2008] showed that despite the large scatter of SCIAMACHY retrievals, and taking retrieval biases into consideration, monthly averages over reasonably large spatial domains showed good agreement with the amplitude and phase of the NH X_{CO2} seasonal cycle as captured by FTS instruments.

[47] Although the global covariance parameters presented in this section clearly show the seasonal cycle of X_{CO2}, X_{CO2} seasonal variability estimated by previous studies cannot be compared directly to the results presented in this section. Unlike the seasonal peak-to-peak amplitude, the global variance parameters presented here are a measure of the spatial variability expected for a given day or month, not temporal variability between months.

4.2. Regional X_{CO2} Variability

[48] The goal of the regional analysis of the spatial structure of X_{CO2} is to reveal patterns of local variability that will be observed by future satellites, and to relate these patterns to differences in the strength of surface fluxes and to seasonal differences in global transport characteristics.

4.2.1. Regional Variance

[49] The regional variance parameters (Figure 3a) show both spatial and temporal variability. The temporal variability is demonstrated by the seasonal change in the magnitude of the regional variances, which follows a seasonal cycle similar to that of the global variance parameters, but with a large range of spatial variability within each month.

[50] The spatial patterns detected by the regional variances include large areas with relatively low variances, representative of background levels of X_{CO2} variability. These variances are approximately 0.5 ppm^2 during the NH winter and spring (November–May), and reach a maximum of 2.5 ppm^2 during the NH summer (June–October).

[51] Areas with higher variance occur over regions with highly variable surface fluxes (e.g., a maximum of 11 ppm^2 over boreal forests in July), and over regions affected by seasonal changes in atmospheric transport (e.g., Arctic and northern ocean during the NH winter) A less prominent role of transport is also apparent during the NH summer when the relatively high variances over the northern tropical Atlantic and North Pacific oceans are caused by flux variability in other regions. In this case, the northern tropical Atlantic is most probably affected by CO_2 variability originating in tropical Africa and southern Europe, and the North Pacific is influenced by CO_2 variability from the southern parts of North America and mid-American continent, which, in both cases, is consistent with the transport pathways established by *Stohl et al.* [2002].

[52] Overall, X_{CO2} regional variance parameters inferred from MATCH/CASA exhibit variability between regions and reflect seasonal fluctuations in regional fluxes and transport. This is clearly shown in the collocation of high variances with, or downwind from, biospherically and anthropogenically active regions. These results support the conclusion that the information scale of retrieved soundings will vary both geographically and seasonally. While some soundings will reflect X_{CO2} over a large region, others will be representative of local variability.

4.2.2. Regional Correlation Lengths

[53] In contrast to the regional variances, the seasonal variability of regional correlation lengths does not show the same seasonal cycle as the global parameters. Figure 3b shows the prevalence of shorter X_{CO2} correlation lengths in the NH for all months (between 200 km and 3000 km on average), relative to the SH. This difference is caused by the limited mixing between the hemispheres and the high spatial variability of the terrestrial fluxes in the NH. The location of the large contrast in correlation lengths reflects the seasonal movement of the ITCZ and is most prominent in June, July and November. The long correlation lengths in the SH are somewhat shorter in August and September, most likely because of the terrestrial tropical fluxes in Africa and South America that introduce spatial variability and cause a drop in correlation lengths over the tropics and the tropical/South Atlantic.

[54] Although regional correlation lengths largely reflect the variability of surface fluxes, their spatial patterns are not as distinct as those of the regional variances. Correlation lengths do seem to reflect large transport-related effects, however. This is apparent in the relatively short correlation lengths in the Polar Regions in general, and in particular the SH. *Olsen and Randerson* [2004] and *Nevison et al.* [2008] point to the potential role of poleward transport of CO_2-enriched or depleted air in elevating the variability in the South Pole region. This is shown in the presented results (Figure 3b) by the decrease in correlation lengths around the South Pole starting in December, becoming shortest in January, and then gradually increasing through April. This reduction corresponds to an increase in the variability of tropical fluxes, thus reinforcing the conclusion that correlation lengths are reflecting large-scale transport. In May, the increasing trend of the SH correlation length is interrupted by a sudden decrease over most of the SH, which marks the transition to the NH summer. This decrease is due to a global reduction in the spatial variability of terrestrial fluxes, which causes a decrease in X_{CO2} variances and correlation lengths.

[55] In general, X_{CO2} regional correlation length parameters reflect more zonal response to changes in surface fluxes relative to the variance parameter. Moreover, correlation lengths show features that reflect global transport of CO_2 variability to the Poles and the lack of mixing between the hemispheres.

4.2.3. Submonthly Temporal Variability

[56] The discussion presented in sections 4.2.1 and 4.2.2 is based on an analysis of the 15th day of each month. The representativeness of this single day of the variability that would be expected for any given day within a certain month is tested by analyzing eight consecutive days in November (13–20 November), which is the month that exhibits the largest within-month change in the global parameters (Figure 2). Results show that the changes in the spatial patterns and magnitudes of the fitted regional parameters are minimal within a 4-day time window, but noticeable differences do occur in the location of the maximum regional variance parameters beyond 4 days. This result indicates that the 15th of each month is an adequate representation of individual days for low-variability months, but that covariance parameters vary on submonthly scales for seasonal transition months. As such, the regional spatial variability analysis may need to be repeated for multiple days within these transition months to capture the temporal changes in the regional spatial variability. This analysis could also be performed using retrieved soundings after the launch of OCO, although some regions may be more difficult to examine because of expected data gaps.

4.2.4. Overall Variability

[57] The parameter h_o provides a single representation of the regional variability of X_{CO2}, as simulated using MATCH-CASA, by translating the seasonal variability in fluxes and transport captured by the regional covariance parameters into regional variability in the spatial scale over which a sounding is representative of local X_{CO2}. Assuming no measurement error or sampling limitations, h_o can also be interpreted as a measure of the relative sounding densities that would be required for achieving global
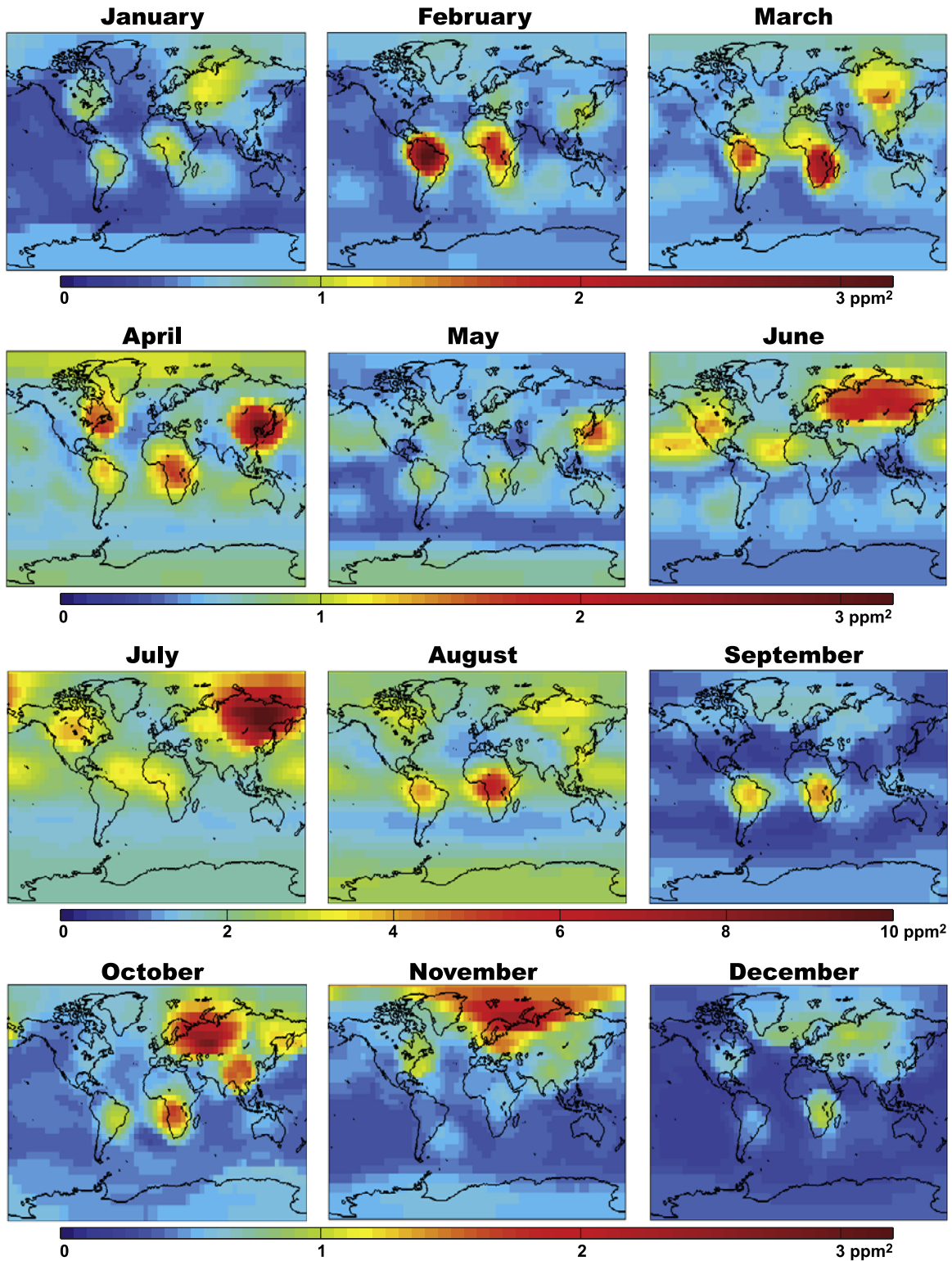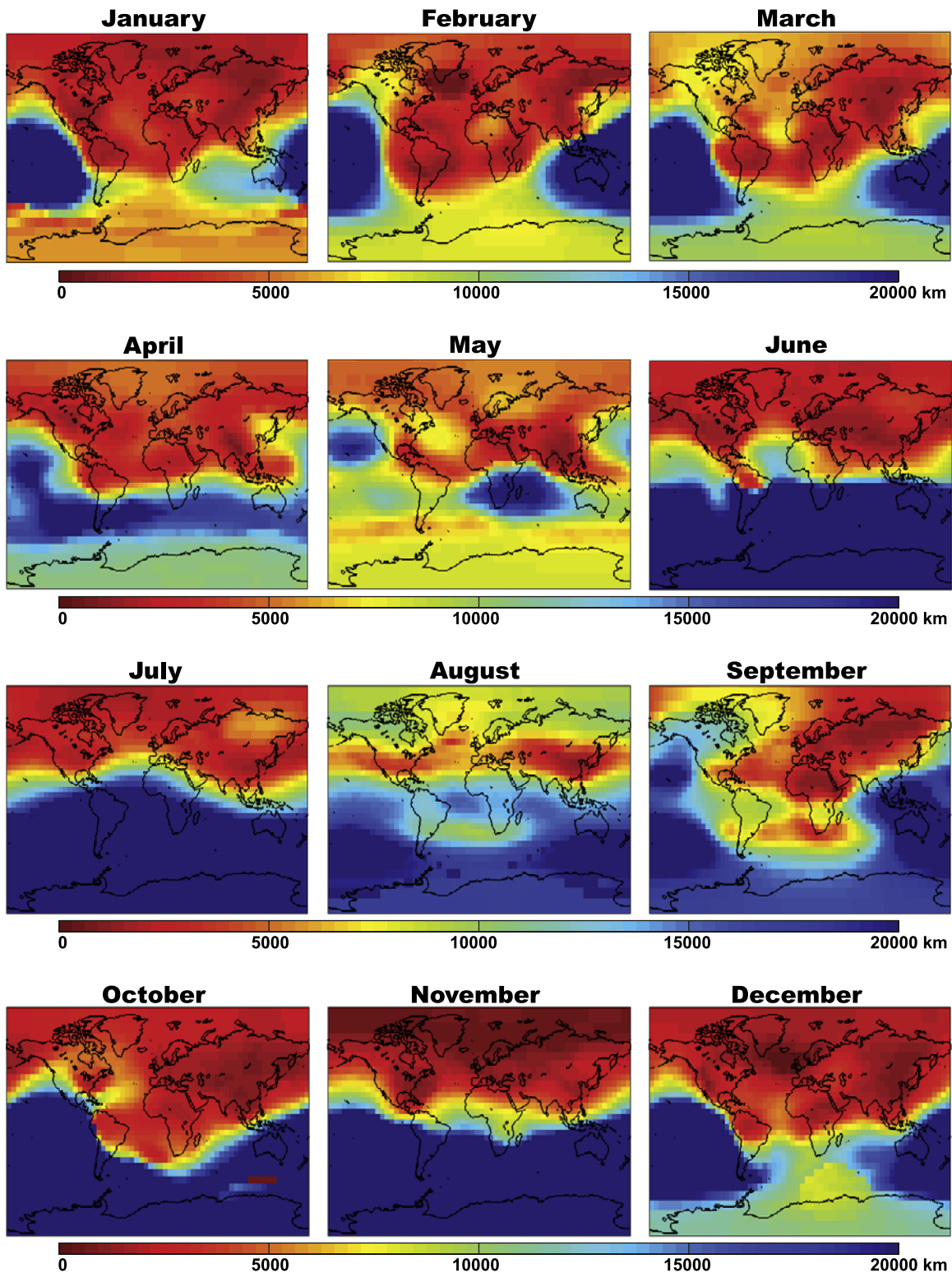
Figure 3a. Regional variance of MATCH/CASA simulated X_{CO2} at 1300 local time on the 15th of each month. Note differences in color scales. Regions are defined as 2000 km radius circles centered at the 2048 MATCH/CASA model grid cells.

X_{CO2} coverage with relatively uniform uncertainty. Figure 4 shows monthly h_o values for a 0.5 ppm uncertainty threshold ($\sqrt{V_{max}}$). In general, h_o varies both spatially and seasonally, and reflects important features in surface flux and transport.

[58] The seasonal changes in the overall variability are most noticeable by observing the maximum regional h_o, which peaks in November and December. h_o values gradually decrease during the following months, reaching a minimum

Figure 3b. Regional correlation length of MATCH/CASA simulated X$_{CO2}$ at 1300 local time on the 15th of each month. Regions are defined as 2000 km radius circles centered at the 2048 MATCH/CASA model grid cells.

in July and August before increasing again in September and October.

[59] The overall variability tends to be higher over continental regions north of the ITCZ (shorter h_o), lower over continental regions south of the ITCZ, and variable over oceans. More specifically, regional h_o values over the NH continents are short for fall, winter and spring. During the NH summer, very high variances cause h_o values to further drop to lengths that are less than half of the MATCH/CASA resolution (i.e., less than 250 km). These
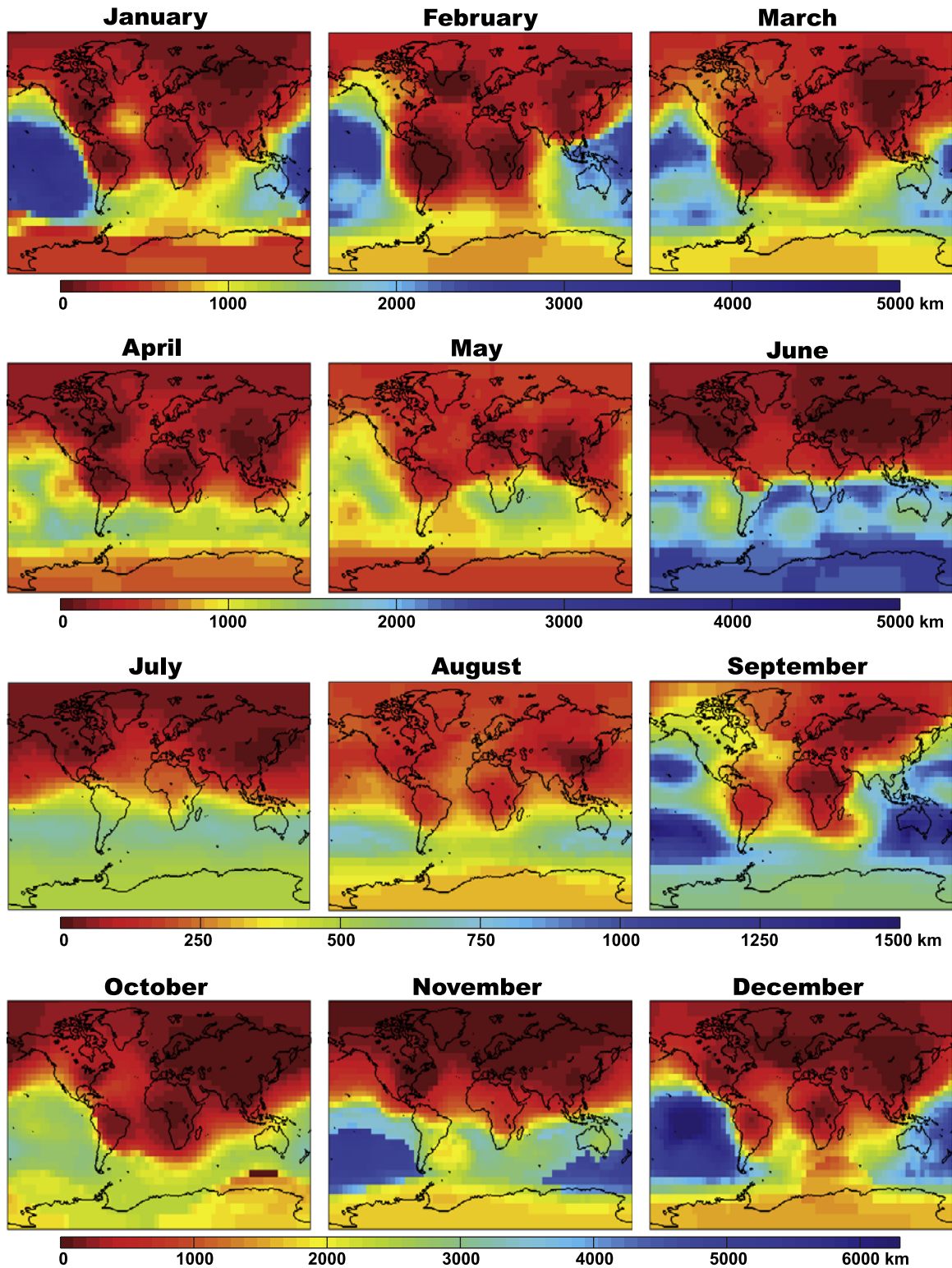
Figure 4. Information scale h_o based on MATCH/CASA regional spatial covariance structure for 0.5 ppm uncertainty level.

results are consistent with the findings of *Karstens et al.* [2006], who analyzed high-resolution (90 km and 55 km) monthly averaged simulated CO_2 concentrations over Europe. This earlier study looked at the distance at which the correlation coefficient between time series of CO_2 concentrations at different locations fell to 0.7. Results of

Karstens et al. [2006] showed maximum separation distances between 170 km and 500 km in the summer, and increasing to 1000 km in the winter.

[60] In contrast to the NH continental regions, Australia shows large h_o values that are more affected by the SH correlation length patterns. Tropical Africa and South

America show short h_o values, which reflect continental fluxes for seasons when the tropics have high variances relative to surrounding regions. During other seasons, h_o values are strongly affected by the location of the ITCZ, with longer h_o values south of the ITCZ.

[61] Oceanic h_o varies greatly between ocean basins, as well as seasonally. The Arctic Ocean shows persistently high variability and therefore low h_o, while the southern Pacific shows persistently lower variability and higher h_o. The north and tropical Atlantic oceans show some seasonality with low h_o comparable to continental values for most of the year, except in December when h_o is much higher. On the other hand, the North Pacific Ocean is highly seasonal with short h_o values varying between values similar to continental regions in June though August, and very long h_o values in December. The Indian Ocean has the strongest seasonality, with h_o ranging between 350 km and 2,000 km during fall and spring, dropping to very low values from July to September and increasing to much longer values in November and December. Finally, the Southern Ocean spatial variability does not show large seasonality, but shows a longitudinal distribution with high h_o values everywhere except between 60°W and 90°E where it shows higher spatial variability.

[62] Although continental X_{CO2} variability is mainly controlled by surface fluxes, variability over the oceans is less controlled by oceanic fluxes because the mixing and transport of the highly variable land fluxes in the averaged CO_2 column cause strong land fluxes to control oceanic X_{CO2} variability near land regions. Furthermore, elevated variability is particularly apparent over coastal regions that include both land and ocean influences. Therefore, overall X_{CO2} variability over oceans does not reflect the variability of underlying ocean fluxes as reported by studies such as *McKinley et al.* [2004]. This study noted that the highest flux variability originates from the Pacific followed by the Southern Ocean, and that the Atlantic exhibits the least flux variability. For the spatial variability analysis presented in this study, the highest overall variability over oceanic regions is over the Atlantic Ocean (particularly the north and tropical), because of the influence of fluxes from North America, Asia, and Europe. The Pacific Ocean shows some seasonality that mostly reflects the seasonal change in the location of the ITCZ and seasonal changes in transported fluxes from Asia, North and South America. These characteristics also support the conclusion that land and not ocean fluxes are the primary control on the variability of X_{CO2} over oceans.

[63] In general, the h_o parameter is used to merge the spatial covariance parameters presented in sections 4.2.1 and 4.2.2 and provides a single representation of X_{CO2} variability. Because this parameter can be defined for any variogram or covariance function, it also serves as an ideal basis for comparison to other models and data presented in the following section. The seasonality of CO_2 surface fluxes and changes in global transport cause the overall X_{CO2} variability over land and ocean areas itself to display significant spatial and temporal variability; therefore indicating that the local X_{CO2} covariance structure must be taken into account when evaluating the spatial representativeness of individual soundings and the uncertainty associated with gap-filled X_{CO2} maps. Finally, the factors controlling this variability go beyond those that control the variability in local surface fluxes, with a strong observed influence of changes in global transport patterns.

4.3. Comparison to Other Models and Aircraft Data

[64] This section tests the robustness of the modeled X_{CO2} spatial covariance structure to (1) changes in X_{CO2} introduced by differences in model setup, transport and CO_2 fluxes and (2) differences between the spatial resolution of MATCH/CASA (5.5°) and the sampling footprints of future satellites (e.g., 3 km² for OCO).

4.3.1. PCTM/GEOS-4 Global Simulation

[65] The spatial variability of X_{CO2} fields modeled using PCTM/GEOS-4 are compared to those from MATCH/CASA to examine whether a higher-resolution model will predict more X_{CO2} variability, and whether the use of assimilated meteorological fields will have a substantial impact on the specific regions exhibiting high variability.

[66] Figure 5 shows regional covariance parameters obtained from the PCTM/GEOS-4 model for January, April, July and October 2002. The range of variances and correlation lengths are very similar to those estimated using the MATCH/CASA model for all four months, implying a relatively low sensitivity of inferred X_{CO2} variability to the increased resolution of PCTM/GEOS-4. This result supports the contention that the MATCH/CASA model is able to represent X_{CO2} variability that is representative of observations taken at finer scales than the model grid. In other words, it begins to point toward the idea that the majority of the variability in X_{CO2} occurs at scales that can be captured by relatively coarse global models.

[67] Figure 5 also shows that for both models, the location and timing of high regional variances correspond to areas with high variability in the surface fluxes due to either fossil fuel emissions or biospheric activity. Nevertheless, there are differences in the magnitude and spatial extent of high-variance regions. The most prominent differences in regional variances occur over (1) eastern Europe in January and October, where MATCH/CASA indicates high variances whereas PCTM/GEOS-4 exhibits lower variances, and (2) Asia, where MATCH/CASA indicates high variances during April and October, while PCTM/GEOS-4 shows high variances over a larger area in January. Although large differences are also found over tropical South America in April, the variability observed in the PCTM/GEOS-4 simulation appears to be dependent on the time of day (results not shown).

[68] Given the similarity of the fluxes prescribed in the two models, differences in the observed location and timing of high-variability regions are mostly attributable to differences in mixing and transport. Nevertheless, some of the observed differences may also be due to differences in submonthly variability in the fluxes imposed in MATCH/CASA versus PCTM/GEOS-4. These conclusions were further validated by analyzing the spatial variability of the prescribed biospheric and fossil fuel fluxes, as well as the spatial variability of X_{CO2} simulations using PCTM/GEOS-4 including only biospheric or fossil fuel fluxes (results not shown).

[69] Correlation lengths of MATCH/CASA and PCTM/GEOS-4 are even more consistent than the variance parameters. The most noticeable differences are the shorter correlation lengths inferred by PCTM/GEOS-4 over the
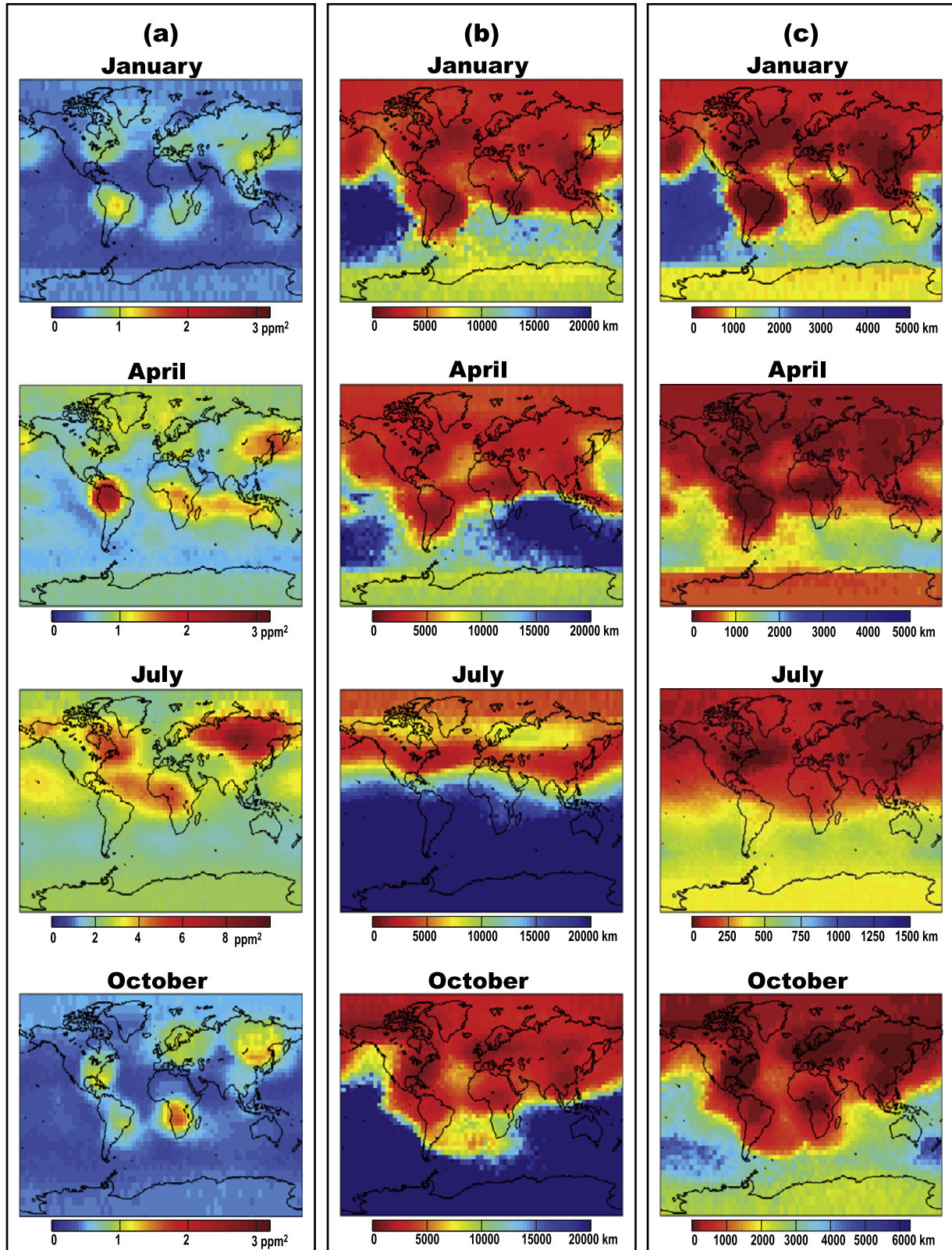
Figure 5. PCTM/GEOS-4 X_{CO_2} (a) regional variance, (b) regional correlation length, and (c) overall information scale (h_o) for 0.5 ppm uncertainty level. All columns are evaluated at 1300 local time on 15 January, 15 April, 15 July, and 15 October.

Table 1. Parameter h_o for Coincident Regions and Periods for MATCH/CASA Global Simulation, PCTM/GEOS-4 Global Simulation, SiB-RAMS Regional Model, and Aircraft Measurements[a]

| Model/Data | Resolution | Column Elevation | h_o Parameter for 0.5 ppm Uncertainty Level (km) | | |
| | | | North America: June–August | Pacific Ocean | |
				February–April	August–October
MATCH/CASA	$5.5° \times 5.5°$	surface to 60 km	85	1200	900
PCTM/GEOS-4	$2.5° \times 2°$	surface to 48 km	70	400	1600
SIB-RAMS	40 km	30 m to 3 km (PBL)	60–90[b]	–	–
SIB-RAMS	40 km	30 m to 9 km	85–140[b]	–	–
SIB-RAMS	40 km	30 m to 21 km	100–150[b]	–	–
SIB-RAMS	40 km	30 m to 60 km	105–160[b]	–	–
Aircraft	point	North America: PBL; Pacific Ocean: 150 m to 3 km	10	70	70
Aircraft	point	150 m to 9 km	5–100[c]	200–750[c]	200–750[c]

[a]Reported h_o values correspond to different months within the indicated range because of data availability.
[b]Range represents h_o variability over 10 day simulation period.
[c]Range represents uncertainty in fitted variogram parameters.

North Pacific and over South America in January and April. Over the North Pacific, differences can be attributed to differences in transport and possibly model resolution, while over South America differences are mostly due to differences in biospheric flux variability. PCTM/GEOS-4 also shows slightly longer correlation lengths over Antarctica in January, which again most likely reflect differences in modeled transport.

[70] More important, however, are the potential effects of these differences on the overall variability as described by the h_o parameter, which represents the information "footprint" of individual measurements (or grid cells). Figures 4 and 5 show that h_o varies over the same range for MATCH/CASA as for PCTM/GEOS-4 (at the 0.5 ppm uncertainty threshold) for all months, with highly consistent regional spatial patterns. Some exceptions occur (1) over the Southern Hemisphere during July, where PCTM/GEOS-4 shows more overall variability (lower h_o), and (2) over the SH oceans during October, where PCTM/GEOS-4 shows less overall variability (longer h_o). This last difference is attributable to an anomaly in the MATCH/CASA simulation over Antarctica for that day (see Figure 3b, October).

[71] Overall, the comparison of the MATCH/CASA model to PCTM/GEOS-4 leads to two main conclusions. First, the consistent range of values in the regional covariance parameters points to a low sensitivity of inferred X_{CO2} spatial variability to a change in model resolution from $5.5° \times 5.5°$ for MATCH/CASA to $2° \times 2.5°$ for PCTM/GEOS-4. Second, despite some differences in the spatial patterns of the regional covariance parameters due to differences in model winds, the overall regional spatial variability as quantified by h_o is highly consistent between the two models. These results support the conclusion that X_{CO2} is a smooth process that varies on large spatial scales, and that the spatial variability inferred from MATCH/CASA may indeed be representative of the variability at smaller scales, as will be observed by satellites such as OCO.

4.3.2. SiB-RAMS Regional Simulation

[72] The SiB-RAMS simulation provides a measure of X_{CO2} spatial variability under conditions that most closely resemble satellite measurements among the three examined models, because (1) the model resolution is closest to the spatial scale of future satellite footprints; (2) the analyzed simulation represents X_{CO2} concentrations over North America in August before and during the passage of a

weather front, which is preceded by large CO_2 fluctuations with surface CO_2 concentrations increasing by up to 40 ppm [*Wang et al.*, 2007]; and (3) the biospheric fluxes in the SiB-RAMS simulation are generated by the model according to the meteorological and biospheric conditions of the simulated time period. Thus, the SiB-RAMS model represents an important validation step for the X_{CO2} spatial variability that will be observed by future satellites.

[73] Table 1 presents the information scale of individual measurements (or grid cells), as represented by the parameter h_o derived from the SiB-RAMS model, and compares these values to those inferred from MATCH/CASA, PCTM/GEOS-4, and aircraft X_{CO2} partial columns. The comparison shows little sensitivity of h_o to the examined differences in model resolution. For example, the average h_o over North America for SiB-RAMS simulation period is 130 km, compared to 85 km for MATCH/CASA. Over the 10-day SiB-RAMS simulation, this parameter ranged from 105 km to 160 km.

[74] Results for individual days of the SiB-RAMS simulation show that the weather front is preceded by an increase in CO_2 variability followed by a decrease during the weather front then a return to initial variability levels of about 110 km. Even during the rapid CO_2 fluctuations, before the passage of the weather front (between 11 and 14 August), h_o values do not vary substantially, indicating that although the concentrations themselves vary in time, the scales of spatial variability remain relatively constant. Therefore, h_o values of MATCH/CASA simulations for North America can capture very similar features in X_{CO2} spatial variability as a model with a 40 km resolution. Note that a 40 km resolution is comparable to the 10 km swath width of the OCO instrument.

[75] Although the variability of spatial processes, such as X_{CO2}, are affected by the measurement scale (i.e., model resolution or satellite footprint) [*Gotway and Young*, 2002; *Skoien and Bloschl*, 2006], the PCTM/GEOS-4 and SiB-RAMS results presented in this study show that model resolution within the examined range is not a major factor controlling the spatial variability in modeled X_{CO2}. Results of this study show that X_{CO2} is a smooth spatial process relative to surface fluxes and concentrations. The smoothness of X_{CO2} explains the low sensitivity of the inferred variability to model resolution, and further supports the contention that the spatial variability inferred from a

relatively coarse global model can be representative of the variability that would be observed at finer scales, and is indicative of the relative scales of variability that will need to be captured by satellites such as OCO. This smoothness relative to surface fluxes and concentrations is caused by the averaging of low variability CO_2 at higher altitudes.

[76] However, given that it is possible that some additional artificial smoothing is also caused by transport effects, errors in mixing parameterization, or errors in flux distributions that are consistent between the examined models, the spatial variabilities predicted by these models are also compared to those derived from in situ measurements in the next section.

4.3.3. Aircraft Data

[77] This section compares the h_o values of MATCH/ CASA to the h_o values calculated using the covariance parameters of X_{CO2} partial columns (<9 km) as reported by *Lin et al.* [2004a]. The comparison is limited to North America and the Pacific Ocean because of the spatial coverage of the aircraft campaigns.

[78] For an uncertainty threshold of 0.5 ppm, the ranges of the power variogram parameter reported by *Lin et al.* [2004a] over North America for June 2003 correspond to h_o with an uncertainty range of 5 km to 100 km. The MATCH/CASA average h_o for the same month and region is 85 km, which is within the uncertainty bounds of the parameter derived from the aircraft data. For the Pacific Ocean (February to April and August to October over several years), the reported covariance parameters correspond to an h_o in the range of 200 km to 750 km. The average MATCH/CASA h_o for the same regions is 1200 km and 900 km in March and September, respectively (Table 1).

[79] In general, the spatial variability observed during the aircraft campaigns and that predicted by MATCH/CASA are consistent over the examined regions. Differences in h_o values, particularly over the Pacific Ocean, during the sampled months can be attributed to three factors. First, in contrast to model simulations, the aircraft data are collected on relatively long time scales. Although *Lin et al.* [2004a] restricted the covariance function calculation to data pairs within a 3-h time window, different pairs would still represent multiple days or different times of the day. Therefore, nonstationary temporal variability captured by the aircraft data may have been interpreted as additional spatial variability. Second, X_{CO2} spatial variability of aircraft data is evaluated using concentrations up to only 9 km in altitude, whereas MATCH/CASA models X_{CO2} up to an elevation of 60 km, which is more comparable to the column that will be observed by future satellites. The effect of increasing the height of the measured column on X_{CO2} spatial variability is demonstrated in Table 1, where the SiB-RAMS h_o value for a 60 km column is about double its value for a 3 km column. The reduced X_{CO2} spatial variability with increasing column elevation is also demonstrated by *Lin et al.* [2004a], who reported variogram parameters corresponding to h_o values that increase as the height of the column increases (Table 1). Thus, the higher X_{CO2} variability observed during the aircraft flights can also be attributed to the aircraft measurement of only partial columns (9 km elevation), with correspondingly higher CO_2 variability, relative to the column that will be measured by OCO and that was modeled by MATCH/CASA. Third, although the observed differences

can be explained by the two factors described above, the higher X_{CO2} spatial variability inferred from aircraft data relative to model simulations could potentially also be caused by actual variability not captured by the highest-resolution model used in this study (SiB-RAMS) or by differences between model fluxes/transport and actual aircraft sampling conditions. If this is the case, future satellites may observe higher X_{CO2} variability than predicted by model simulations, but this last possibility cannot be tested using the limited available data.

[80] Overall, the comparison of X_{CO2} variability inferred from the various models and aircraft data supports the conclusion that the scales of variability inferred using the MATCH/CASA model are representative of those that will be observed by satellites such as OCO. The analyses performed using PCTM/GEOS-4 and SiB-RAMS demonstrate the robustness of the estimates described in section 4.2 to a range of model resolutions and setups. The comparison to aircraft data demonstrates the consistency of the estimates with observed variability. One caveat that must be taken into account, and that cannot be resolved given the current limited availability of column-integrated measurements, is the remaining possibility that model simulations cannot reproduce some of the small-scale variability that will be observed by future satellites with small measurement footprints (e.g., 3 km^2 for the OCO). This is due to the high uncertainty in X_{CO2} spatial variability inferred from aircraft measurements, which prevents a definite conclusion on this question. Nevertheless, the presented results provide strong evidence that the smoothness of the X_{CO2} signal means that models that would be too coarse to resolve variability in surface CO_2 concentrations may indeed be able to adequately capture variability in the integrated X_{CO2} signal. In addition, the presented results demonstrate that the predominant spatial patterns in the variability of X_{CO2} are consistent between models, as well as for available field data, and that these patterns are attributable both to variability in the underlying flux distribution, and regional and seasonal variability in global transport.

5. Conclusions

[81] Understanding of the spatial variability of X_{CO2}, as well as the seasonality and regional differences in this variability, is necessary for making optimal use of the data that will be provided by satellites such as OCO. The evaluated spatial variability facilitates the use of spatial interpolation methods to (1) gap fill the retrieved soundings and evaluate the uncertainty associated with gap-filled data products; (2) quantify the representation errors associated with incorporating X_{CO2} into atmospheric transport models or GCMs when the model resolution differs from the satellite footprint; and (3) in the case of computational limitations, design a sounding selection algorithm that captures the underlying spatial variability of the X_{CO2} field.

[82] In this study, the regional X_{CO2} spatial covariance structure is inferred using global X_{CO2} distributions simulated using the MATCH/CASA model. The evaluated spatial variability is compared to that inferred from a second higher-resolution global model, a regional model, and aircraft measurements. Results show that the degree of observed spatial variability is consistent among the examined models,

and robust at spatial resolutions down to 40 km. Results are also consistent with variability inferred from aircraft measurements. Together, these results support the conclusion that the spatial variability inferred using the MATCH/CASA model is representative of the variability of X_{CO2} as will be observed at much finer footprints. Because the X_{CO2} signal is very diffuse relative to surface CO_2 concentrations, relatively coarse global models are able to represent the expected degree of X_{CO2} spatial variability at smaller scales.

[83] The presented analysis shows that both the variance and correlation lengths of the X_{CO2} field vary spatially and seasonally, and that this variability is attributable to changes in both surface fluxes and seasonal patterns in global transport. The variance parameter shows a clear cycle that reflects the NH growing season with peak values collocated with regions of highly variable CO_2 surface fluxes. The effect of transport on the variance parameter is clearest during the NH winter months, when highly variable fluxes from NH continents are transported to the Arctic and northern ocean. The correlation lengths of the X_{CO2} field, on the other hand, do not show a distinct seasonal cycle, but clearly reflect transport and mixing effects. These effects are demonstrated by the contrast in correlation lengths between the hemispheres, and the effects of the seasonal movement of the ITCZ on the boundary between regions with low and high correlation lengths.

[84] Overall X_{CO2} spatial variability is quantified using the parameter h_o, which represents the relative spatial scale of the information provided by a single X_{CO2} observation in a given region. h_o values vary between hemispheres and between ocean and continental regions. Values are lowest during the NH summer over highly active continental flux areas, and are highest over the Pacific Ocean during the NH winter. The X_{CO2} variability over the oceans, particularly near continental regions, is primarily controlled by transport of CO_2 signals from continental regions.

[85] Results are consistent with the conclusion that a spatially and temporally variable sounding density would be required to capture the regional differences in the spatial variability of X_{CO2} with a uniform precision. Moreover, the representativeness of individual soundings is expected to vary regionally and seasonally, as a function of the heterogeneity in the identified spatial variability, with soundings from high-variability regions having higher representation errors when used to represent X_{CO2} in coarser models.

[86] Geophysical limitations (e.g., clouds, aerosol) and instrument characteristics (e.g., satellite track) are expected to cause large gaps in retrieved X_{CO2} distributions, and computational costs may further limit the fraction of retrieved soundings in the early parts of the OCO mission. The evaluated X_{CO2} variability provides important information about the ability of future satellites to capture the underlying X_{CO2} distribution given these limitations. For example, given the maximum 2500 km coverage gap of consecutive orbits of OCO at the equator, and discounting all other sampling limitations, this analysis suggest gap-filling uncertainties that closely follow the patterns seen in the variance maps (Figure 3a), reaching a maximum of 4 ppm over boreal Asia in July, and with generally low values (<1 ppm) over oceans and regions with low surface flux variability (detailed results not shown).

[87] Finally, the analysis presented in this paper establishes the main patterns of X_{CO2} spatial variability and how surface fluxes and transport affect these patterns as simulated by current models. Because these models reflect the current scientific understanding of surface fluxes of CO_2, the results also provide a baseline for evaluating the contribution of future satellites in improving the present understanding of the X_{CO2} distribution and its spatiotemporal variability.

References

Alkhaled, A., A. M. Michalak, and S. R. Kawa (2008), Using CO_2 spatial variability to quantify representation errors of satellite CO_2 retrievals, *Geophys. Res. Lett.*, *35*, L16813, doi:10.1029/2008GL034528.

Andres, R. J., G. Marland, I. Fung, and E. Matthews (1996), A 1° × 1° distribution of carbon dioxide emissions from fossil fuel consumption and cement manufacture, 1950−1990, *Global Biogeochem. Cycles*, *10*, 419−429, doi:10.1029/96GB01523.

Barkley, M. P., P. S. Monks, and R. J. Engelen (2006a), Comparison of SCIAMACHY and AIRS CO_2 measurements over North America during the summer and autumn of 2003, *Geophys. Res. Lett.*, *33*, L20805, doi:10.1029/2006GL026807.

Barkley, M. P., P. S. Monks, U. Friess, R. L. Mittermeier, H. Fast, S. Korner, and M. Heimann (2006b), Comparisons between SCIAMACHY atmospheric CO_2 retrieved using (FSI) WFM-DOAS to ground based FTIR data and the TM3 chemistry transport model, *Atmos. Chem. Phys.*, *6*, 4483−4498.

Barkley, M. P., et al. (2007), Assessing the near surface sensitivity of SCIAMACHY atmospheric CO_2 retrieved using (FSI) WFM-DOAS, *Atmos. Chem. Phys.*, *7*, 3597−3619.

Bösch, H., et al. (2006), Space-based near-infrared CO_2 measurements: Testing the Orbiting Carbon Observatory retrieval algorithm and validation concept using SCIAMACHY observations over Park Falls, Wisconsin, *J. Geophys. Res.*, *111*, D23302, doi:10.1029/2006JD007080.

Buchwitz, M., et al. (2005), Carbon monoxide, methane and carbon dioxide columns retrieved from SCIAMACHY by WFM-DOAS: Year 2003 initial data set, *Atmos. Chem. Phys.*, *5*, 3313−3329.

Buchwitz, M., O. Schneising, J. P. Burrows, H. Bovensmann, M. Reuter, and J. Notholt (2007), First direct observation of the atmospheric CO_2 year-to-year increase from space, *Atmos. Chem. Phys.*, *7*, 5341−5342.

Chevallier, F., F. M. Breon, and P. J. Rayner (2007), Contribution of the Orbiting Carbon Observatory to the estimation of CO_2 sources and sinks: Theoretical study in a variational data assimilation framework, *J. Geophys. Res.*, *112*, D09307, doi:10.1029/2006JD007375.

Chiles, J.-P., and P. Delfiner (1999), *Geostatistics: Modeling Spatial Uncertainty*, John Wiley, New York.

Conway, T. J., P. P. Tans, L. S. Waterman, and K. W. Thoning (1994), Evidence for interannual variability of the carbon cycle from the National Oceanic and Atmospheric Administration/Climate Monitoring and Diagnostics Laboratory Global Air Sampling Network, *J. Geophys. Res.*, *99*(D11), 22,831−22,855.

Corbin, K. D., A. S. Denning, L. Lu, J. W. Wang, and I. T. Baker (2008), Possible representation errors in inversions of satellite CO_2 retrievals, *J. Geophys. Res.*, *113*, D02301, doi:10.1029/2007JD008716.

Cressie, N. A. C. (1993), *Statistics for Spatial Data*, 900 pp., John Wiley, New York.

Crisp, D., et al. (2004), The Orbiting Carbon Observatory (OCO) mission, *Adv. Space Res.*, *34*, 700−709, doi:10.1016/j.asr.2003.08.062.

Denning, A. S., M. Nicholls, L. Prihodko, I. Baker, P. L. Vidale, K. Davis, and P. Bakwin (2003), Simulated variations in atmospheric CO_2 over a

Wisconsin forest using a coupled ecosystem-atmosphere model, *Global Change Biol.*, 9, 1241–1250, doi:10.1046/j.1365-2486.2003.00613.x.

Doney, S. C., D. M. Glover, S. J. McCue, and M. Fuentes (2003), Mesoscale variability of Sea-viewing Wide Field-of-view Sensor (SeaWiFS) satellite ocean color: Global patterns and spatial scales, *J. Geophys. Res.*, 108(C2), 3024, doi:10.1029/2001JC000843.

Engelen, R. J., and A. P. McNally (2005), Estimating atmospheric CO_2 from advanced infrared satellite radiances within an operational four-dimensional variational (4D-Var) data assimilation system: Results and validation, *J. Geophys. Res.*, 110, D18305, doi:10.1029/2005JD005982.

Geels, C., S. C. Doney, R. Dargaville, J. Brandt, and J. H. Christensen (2004), Investigating the sources of synoptic variability in atmospheric CO_2 measurements over the Northern Hemisphere continents: A regional model study, *Tellus, Ser. B*, 56, 35–50, doi:10.1111/j.1600-0889.2004.00084.x.

Gerbig, C., J. C. Lin, S. C. Wofsy, B. C. Daube, A. E. Andrews, B. B. Stephens, P. S. Bakwin, and C. A. Grainger (2003a), Toward constraining regional-scale fluxes of CO_2 with atmospheric observations over a continent: 1. Observed spatial variability from airborne platforms, *J. Geophys. Res.*, 108(D24), 4756, doi:10.1029/2002JD003018.

Gerbig, C., J. C. Lin, S. C. Wofsy, B. C. Daube, A. E. Andrews, B. B. Stephens, P. S. Bakwin, and C. A. Grainger (2003b), Toward constraining regional-scale fluxes of CO_2 with atmospheric observations over a continent: 2. Analysis of COBRA data using a receptor-oriented framework, *J. Geophys. Res.*, 108(D24), 4757, doi:10.1029/2003JD003770.

GLOBALVIEW-CO_2 (2005), Cooperative Atmospheric Data Integration Project–Carbon Dioxide [CD-ROM], Earth Syst. Res. Lab., NOAA, Boulder, Colo. (Available at ftp://ftp.cmdl.noaa.gov/ccg/co2/GLOBALVIEW)

Gotway, C. A., and L. J. Young (2002), Combining incompatible spatial data, *J. Am. Stat. Assoc.*, 97, 632–648, doi:10.1198/016214502760047140.

Karstens, U., M. Gloor, M. Heimann, and C. Rodenbeck (2006), Insights from simulations with high-resolution transport and process models on sampling of the atmosphere for constraining midlatitude land carbon sinks, *J. Geophys. Res.*, 111, D12301, doi:10.1029/2005JD006278.

Kawa, S. R., D. J. Erickson, S. Pawson, and Z. Zhu (2004), Global CO_2 transport simulations using meteorological data from the NASA data assimilation system, *J. Geophys. Res.*, 109, D18312, doi:10.1029/2004JD004554.

Law, R. M., et al. (2008), TransCom model simulations of hourly atmospheric CO_2: Experimental overview and diurnal cycle results for 2002, *Global Biogeochem. Cycles*, 22, GB3009, doi:10.1029/2007GB003050.

Lin, J. C., C. Gerbig, B. C. Daube, S. C. Wofsy, A. E. Andrews, S. A. Vay, and B. E. Anderson (2004a), An empirical analysis of the spatial variability of atmospheric CO_2: Implications for inverse analyses and space-borne sensors, *Geophys. Res. Lett.*, 31, L23104, doi:10.1029/2004GL020957.

Lin, J. C., C. Gerbig, S. C. Wofsy, A. E. Andrews, B. C. Daube, C. A. Grainger, B. B. Stephens, P. S. Bakwin, and D. Y. Hollinger (2004b), Measuring fluxes of trace gases at regional scales by Lagrangian observations: Application to the CO_2 Budget and Rectification Airborne (COBRA) study, *J. Geophys. Res.*, 109, D15304, doi:10.1029/2004JD004754.

Lu, L. X., A. S. Denning, M. A. da Silva-Dias, P. da Silva-Dias, M. Longo, S. R. Freitas, and S. Saatchi (2005), Mesoscale circulations and atmospheric CO_2 variations in the Tapajos Region, Para, Brazil, *J. Geophys. Res.*, 110, D21102, doi:10.1029/2004JD005757.

McKinley, G. A., C. Rodenbeck, M. Gloor, S. Houweling, and M. Heimann (2004), Pacific dominance to global air-sea CO_2 flux variability: A novel atmospheric inversion agrees with ocean models, *Geophys. Res. Lett.*, 31, L22308, doi:10.1029/2004GL021069.

McNeal, R. J. (1983), NASA Global Tropospheric Experiment, *Eos Trans. AGU*, 64, 561–562.

Miller, C. E., et al. (2007), Precision requirements for space-based X$_{CO_2}$ data, *J. Geophys. Res.*, 112, D10314, doi:10.1029/2006JD007659.

National Institute for Environmental Studies (2006), GOSAT: Greenhouse Gases Observing Satellite, *Tsukuba, Japan*.

Nevison, C. D., et al. (2008), Contribution of ocean, fossil fuel, land biosphere, and biomass burning carbon fluxes to seasonal and interannual variability in atmospheric CO_2, *J. Geophys. Res.*, 113, G01010, doi:10.1029/2007JG000408.

Nicholls, M. E., A. S. Denning, L. Prihodko, P. L. Vidale, I. Baker, K. Davis, and P. Bakwin (2004), A multiple-scale simulation of variations in atmospheric carbon dioxide using a coupled biosphere-atmospheric model, *J. Geophys. Res.*, 109, D18117, doi:10.1029/2003JD004482.

Olsen, S. C., and J. T. Randerson (2004), Differences between surface and column atmospheric CO_2 and implications for carbon cycle research, *J. Geophys. Res.*, 109, D02301, doi:10.1029/2003JD003968.

Randerson, J. T., M. V. Thompson, T. J. Conway, I. Y. Fung, and C. B. Field (1997), The contribution of terrestrial sources and sinks to trends in the seasonal cycle of atmospheric carbon dioxide, *Global Biogeochem. Cycles*, 11, 535–560, doi:10.1029/97GB02268.

Rayner, P. J., and D. M. O'Brien (2001), The utility of remotely sensed CO_2 concentration data in surface source inversions, *Geophys. Res. Lett.*, 28, 175–178, doi:10.1029/2000GL011912.

Schneising, O., M. Buchwitz, J. P. Burrows, H. Bovensmann, M. Reuter, J. Notholt, R. Macatangay, and T. Warneke (2008), Three years of greenhouse gas column-averaged dry air mole fractions retrieved from satellite—Part 1: Carbon dioxide, *Atmos. Chem. Phys.*, 8, 3827–3853.

Shia, R. L., M. C. Liang, C. E. Miller, and Y. L. Yung (2006), CO_2 in the upper troposphere: Influence of stratosphere-troposphere exchange, *Geophys. Res. Lett.*, 33, L14814, doi:10.1029/2006GL026141.

Skoien, J. O., and G. Bloschl (2006), Scale effects in estimating the variogram and implications for soil hydrology, *Vadose Zone J.*, 5, 153–167, doi:10.2136/vzj2005.0069.

Stephens, B. B., et al. (2007), Weak northern and strong tropical land carbon uptake from vertical profiles of atmospheric CO_2, *Science*, 316, 1732–1735, doi:10.1126/science.1137004.

Stohl, A. (Ed.) (2004), *Inter-continental Transport of Air Pollution*, Springer, Berlin.

Stohl, A., S. Eckhardt, C. Forster, P. James, and N. Spichtinger (2002), On the pathways and timescales of intercontinental air pollution transport, *J. Geophys. Res.*, 107(D23), 4684, doi:10.1029/2001JD001396.

Takahashi, T., R. H. Wanninkhof, R. A. Feely, R. F. Weiss, D. W. Chipman, N. Bates, J. Olafsson, C. Sabine, and S. C. Sutherland (1999), Net sea-air CO_2 flux over the global oceans: An improved estimate based on the sea-air pCO₂ difference, paper presented at 2nd CO_2 in Oceans Symposium, Cent. for Global Environ. Res., Natl. Inst. for Environ. Stud., Tsukuba, Japan.

Tiwari, Y. K., et al. (2006), Comparing CO_2 retrieved from Atmospheric Infrared Sounder with model predictions: Implications for constraining surface fluxes and lower-to-upper troposphere transport, *J. Geophys. Res.*, 111, D17106, doi:10.1029/2005JD006681.

Wang, J. W., A. S. Denning, L. X. Lu, I. T. Baker, K. D. Corbin, and K. J. Davis (2007), Observations and simulations of synoptic, regional, and local variations in atmospheric CO_2, *J. Geophys. Res.*, 112, D04108, doi:10.1029/2006JD007410.

Warneke, T., et al. (2005), Seasonal and latitudinal variations of column averaged volume-mixing ratios of atmospheric CO_2, *Geophys. Res. Lett.*, 32, L03808, doi:10.1029/2004GL021597.

Washenfelder, R. A., et al. (2006), Carbon dioxide column abundances at the Wisconsin Tall Tower site, *J. Geophys. Res.*, 111, D22305, doi:10.1029/2006JD007154.

Yang, Z., R. A. Washenfelder, G. Keppel-Aleks, N. Y. Krakauer, J. T. Randerson, P. P. Tans, C. Sweeney, and P. O. Wennberg (2007), New constraints on Northern Hemisphere growing season net flux, *Geophys. Res. Lett.*, 34, L12807, doi:10.1029/2007GL029742.

————————————

A. A. Alkhaled and A. M. Michalak, Department of Civil and Environmental Engineering, University of Michigan, Ann Arbor, MI 48109, USA. (alanood@umich.edu; amichala@umich.edu)

S. R. Kawa, NASA Goddard Space Flight Center, Greenbelt, MD 20771, USA.

S. C. Olsen, Los Alamos National Laboratory, EES-6 MS D462, Los Alamos, NM 87545, USA.

J.-W. Wang, Cooperative Institute for Research in the Environmental Sciences, University of Colorado, Boulder, CO 80309-0216, USA.